

Investigation of Ethylisopropyl Sulfone Medium with a Copper-Based Redox Electrolyte for Ambient Light Dye-Sensitized Solar Cells: Achieving High Efficiency and Enduring Long-Term Stability

Daniela Sayah and Tarek H. Ghaddar*

Cite This: *ACS Appl. Energy Mater.* 2023, 6, 11924–11933

Read Online

ACCESS |

Metrics & More

Article Recommendations

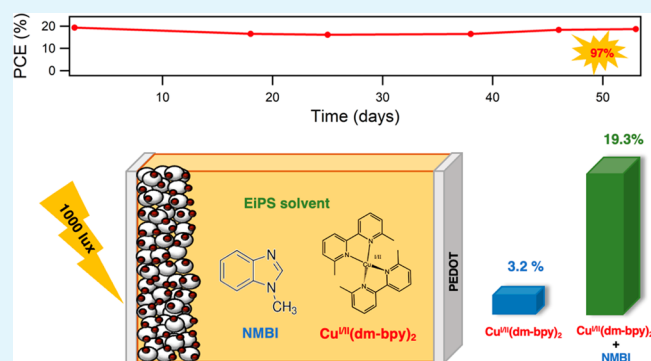
Supporting Information

ABSTRACT: In recent years, dye-sensitized solar cells (DSCs) have shown remarkable efficiency levels, particularly under low light conditions, making them promising candidates for indoor applications. However, for these devices to be successfully commercialized, high power conversion efficiencies (PCEs) alone are not sufficient. Long-term stability is a critical aspect that needs to be addressed. Most of the well performing DSCs reported so far have utilized conventional organic solvents, which have low boiling points and are highly volatile. While these solvents contribute to achieving high PCE values, they are prone to leakage and evaporation, limiting the long-term stability of the devices. Herein, we report on cosensitized DSC devices (A–E) with commercial dyes (XY1b/MSS) and different additives. This was accomplished by employing for the first time ethylisopropyl sulfone (EiPS) as a high boiling point solvent along with $\text{Cu}^{\text{I}}(\text{dmby})_2 \cdot \text{TFMSI}$ and $\text{Cu}^{\text{II}}(\text{dmby})_2 \cdot \text{Cl} \cdot \text{TFMSI}$ as the redox mediators in DSCs. Remarkably, most of the tested DSC devices exhibited exceptional performance, achieving high PCE values ranging from 19% to 23% under 1000 lx irradiation and up to 0.82% under 1 sun simulated solar light irradiation. Our analysis revealed that the *N*-methylbenzimidazole (NMBI) additive played a crucial role in ensuring both good PCE% and long-lasting durability, particularly in device B. On the other hand, the use of additives such as 1-butyl-3-methylimidazolium bis(trifluoromethylsulfonyl)imide (ImTFMSI) and/or LiTFMSI resulted in deterioration of the photovoltaic parameters during the long-term stability tests in the EiPS-based electrolyte medium, observed in devices C–E. This knowledge opens up possibilities for further optimization of ambient-light DSCs with improved stability and provides a viable solution for indoor power generation applications.

KEYWORDS: dye sensitized solar cell, ethylisopropyl sulfone, copper electrolyte, long-term stability, ambient light

INTRODUCTION

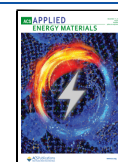
Over the past three decades, research groups around the world have continuously developed and optimized dye-sensitized solar cells (DSCs) due to their appealing properties, which include easy fabrication, acceptable conversion efficiency, and low cost.¹ Significant progress has been made in the field of DSC through the optimization of various components, especially dyes,^{2,3} counter electrodes,^{4,5} and redox mediators.⁶ Recent research has found that DSCs operate efficiently under ambient light conditions and exhibit outstanding power conversion efficiency (PCE) values. This is due to the narrower light spectrum of artificial light, which mainly involves the visible region.^{7,8} In fact, Grätzel et al. have recently demonstrated that DSCs operating under ambient conditions outperform most of the well-known solar cell devices. In their article, they reported an outstanding PCE value of 34.5%, which surpasses the performance of other solar cells such as metal halide perovskite (30.6%), organic polymers (26.1%), GaAs (21%), and amorphous silicon (10.9%).⁹ This



has further sparked research interest in DSCs that operate under low light conditions and in exploring ways to enhance their performance and long-term stability.

Indeed, several studies have been conducted in this regard, with the I^-/I_3^- redox mediator under ambient light achieving PCEs higher than 28%.^{10,11} Additionally, DSCs that operate using cobalt-based redox mediators have been reported with PCEs ranging between 18% and 25% under 1000 lx illumination.^{12,13} However, DSCs with copper-based electrolytes have demonstrated the highest PCE% values up to 38% and V_{oc} values above 1.0 V under low light conditions.^{14–16}

Received: August 17, 2023
Revised: October 9, 2023
Accepted: November 2, 2023
Published: November 17, 2023



As such, DSCs have shown exceptional performance under low light conditions, especially with copper redox mediators. However, for commercialization purposes, it is crucial to evaluate their long-term durability. Unfortunately, there are limited research publications available that investigate the stability of DSCs that are designed for ambient light applications, and most of these studies utilize acetonitrile (ACN), a low-boiling point solvent, in their preparation processes,^{9,13,17–22} while to the best of our knowledge only three reports^{23–25} mention the use of 3-methoxypropionitrile (MPN), a high boiling point solvent, as a substitute solvent when testing under ambient light conditions to improve the device's durability. Thus, it is evident that high-efficiency DSCs often rely on electrolytes based on volatile solvents, as these typically produce exceptional efficiencies with most redox mediators but lack the necessary long-term stability due to evaporation over time.²⁶ Hence, researchers have explored various alternatives to tackle the stability issue in DSCs. One of the initial choices was to investigate quasi-solid-based DSCs (QS-DSCs) which have gained significant attention as a viable alternative to liquid electrolytes for enhancing durability.^{27–31} These DSCs are known for their comparable PCE values to those of liquid electrolytes, coupled with improved stability achieved through the prevention of leakage and evaporation issues. Many research groups have focused on QS-DSCs utilizing I^-/I^{3-} redox mediators tested under 1 sun, benefiting from the negligible mass transport problem in such a redox mediator.^{27,31} However, recently, a few groups have ventured into employing both copper and cobalt redox mediators in QS-DSCs.^{28,30} These experiments have been conducted not only under standard 1 sun conditions but also under indoor low light conditions. This expanded exploration became possible due to the negligible mass transport limitations when testing QS-DSCs under ambient light conditions.

Additionally, there is use of solvents with high boiling points, such as sulfones. Sulfones have emerged as an attractive solution for enhancing stability in DSCs, owing to their desirable properties, such as their high boiling point, excellent electrochemical stability, and not generating gases upon decomposition (with a dielectric constant $\kappa = 55$ and viscosity $\eta = 5.6$ mPa.s at 25°C).³² Several research groups have explored the use of sulfone-based I^-/I^{3-} electrolyte systems in DSCs under 1 sun illumination conditions but there has been limited exploration of copper- or cobalt-based redox systems in this context.^{32–35} The latter can be attributed to potential mass transfer problems associated with such bulkier complexes compared to I^-/I^{3-} , especially when tested under high light intensities of 1 sun (100 mW·cm⁻² or ~100 000 lx). These challenges arise due to the higher viscosities of sulfones as compared to ACN, with sulfones typically exhibiting viscosities exceeding 5 mPa.s at RT. However, such limitations may not be as significant when DSCs are irradiated with low light levels.³⁶ Hence, it is crucial to focus not only on developing a highly efficient DSC but also on ensuring its long-term stability. In this study, we delved into sulfone-based electrolyte systems, incorporating high-performing polypyridyl copper redox couples and various additives in DSCs. These devices were meticulously tested under low-light conditions, and their long-term stability was thoroughly evaluated.

EXPERIMENTAL SECTION

Materials and Instrumentation. All chemicals used in the synthesis of the copper complexes, Cu^I(dmby)₂·TFMSI and

Cu^{II}(dmby)₂Cl·TFMSI using reported methods in the literature,³⁷ were purchased from Sigma-Aldrich (Germany) and used as supplied. The titania pastes (30NR-D Transparent and WER2-O Reflector titania pastes) and EiSP were purchased from Dyesol (Australia). The dyes XY1 and MSS were purchased from Dyenamo (Sweden). Fluorine-doped tin oxide (FTO) transparent conducting glasses “Tec 8” and “Tec 15” were purchased from Pilkington (USA).

All of the electrochemical measurements were performed with a CH Instruments 760E bipotentiostat (USA). Electrochemical impedance spectra (EIS) of the DSCs were performed at V_{OC} under different light levels illumination for the DSCs and at 0 V for the dummy cells in the frequency range 0.1–10⁵ Hz with oscillation potential amplitude of 10 mV at RT. The obtained impedance spectra were fitted with the Z-view software (v2.8b, Scribner Associates Inc.). The Mott–Schottky experiments of undyed DSCs with the various electrolytes were performed at a frequency of 1 kHz and an oscillation potential amplitude of 10 mV at RT.

Photocurrent vs photovoltage characteristics of the DSCs under low light conditions were measured with a Keithley 2400 source meter and light power of 1000 lx from an 18 W Osram T8/930 fluorescent tube. The spectrum and power of the warm white light were measured with a StellarRad spectroradiometer (Stellar Inc., USA), and the illumination power was cross-checked with TES 1334A and Extech LT45 light meters. The average of the photovoltaic parameters of at least three different DSCs are reported after a minimum period of 24 h from the time of cell assembly except when the time is specified in the text.

The photoinduced absorption (PIA) spectra were recorded on a DN-AE02 setup (Dyenamo, Sweden) over a wavelength range of 500–1000 nm after an on/off photomodulation using a 9 Hz blue LED excitation. White probe light from a tungsten-halogen lamp (20 W) was used as an illumination source. The light was focused onto the sample and then to an automated monochromator (Newport, USA) and detected using a silicon photodiode detector.

Solar Cell Fabrication. Dye sensitized solar cells were fabricated using standard procedures. A compact TiO₂ blocking layer was deposited using a pretreatment process with 40 mM TiCl₄ aqueous solution at 70 °C for 1 h followed by sintering at 500 °C for 30 min. A 6 μm mesoporous layer of TiO₂ was then printed on the glass by the doctor-blade method from a titania paste (TiO₂ Dyesol 30NR-D) and sintered on a hot plate with ramped temperatures at 125, 250, 325, 450, and 500 °C for 5, 5, 5, 15, and 30 min, respectively. This was followed by depositing a 6 μm Dyesol WER2-O TiO₂ paste scattering layer and sintering at 500 °C for 30 min. Finally, a post-treatment process with a 40 mM TiCl₄ aqueous solution at 70 °C for 30 min was performed, followed by a sintering process at 500 °C for 30 min and cooling to around 80 °C before immersion into the dye solution. The dye solution was 0.05 mM MSS, 0.1 mM XY1b, and 0.5 mM chenodeoxycholic acid in 1:9 chloroform:ethanol. The PEDOT counter electrodes were prepared by electropolymerization of the EDOT (3,4-ethylenedioxythiophene) monomer (0.01 M EDOT and 0.1 M LiClO₄) onto clean Tec 8 electrodes by a constant applied potential technique at 1.03 V versus Ag/AgCl for 20 to 30 s. Solar cell assembly was done by sealing the counter electrode to the TiO₂ working electrode using a 25 μm Surlyn (Dupont) spacer at ~100 °C for 90 s, followed by introducing the electrolyte, composed of an optimized amount of Cu^I(dmby)₂·TFMSI (0.1 M) and Cu^{II}(dmby)₂Cl·TFMSI (0.05 M) in ethylisopropyl sulfone (EiSP), through predrilled holes and finally sealed with a 2-part epoxy glue. The optimized concentrations of the other additives such as *N*-methylbenzimidazole (NMBI), the ionic liquid 1-butyl-3-methylimidazolium bis(trifluoromethylsulfonyl)imide (ImTFMSI), and LiTFMSI were used with concentrations of 0.6 M, 0.34 M (10% v/v), and 0.1 M when needed, respectively. Dyes' loadings measurements were performed by desorbing a cosensitized 1 × 1 cm² titania film with XY1b and MSS in 10 mL of 0.1 M NaOH solution in 1:9 water:tetrahydrofuran (H₂O:THF) solution and measuring the absorption spectrum of the solution. The individual dye's loading amounts were extracted from the fit of the absorption spectrum using the measured extinction coefficients of both dyes in THF (for XY1b ϵ

= 36 500 M⁻¹·cm⁻¹ at 534 nm, and $\epsilon = 12\,600\text{ M}^{-1}\cdot\text{cm}^{-1}$ at 452 nm for MSS).

RESULTS AND DISCUSSION

In this study, we selected the chemically inert ethylisopropyl sulfone (EiPS) as the DSC's electrolyte polar-solvent due to its high boiling and low vapor pressure (bp 265 °C) that could result in long-term stable and durable DSCs.³⁸ EiPS has been extensively used as the solvent of choice in electric double layer capacitors (EDLCs)³⁸ and in iodide/triiodide based DSCs;^{32,33} however and to the best of our knowledge, sulfones have never been investigated in copper-based DSCs. The organic dyes XY1b and MSS were utilized to prepare cosensitized DSCs (Scheme S1) due to their superb performance when used with copper-based electrolyte system in acetonitrile, especially under ambient light conditions.⁹ The copper(I/II) complexes of 6,6'-dimethyl-2,2'-bipyridine, Cu^{I/II}(dmby)₂(x)TFMSI, were selected as the electrolyte components based mainly on the idea of attaining a high photovoltage (V_{OC}) of the DSC, due to its high redox potential that was determined to be $E_{1/2} = 0.94\text{ V vs NHE}$ ($E_{1/2} = 0.32\text{ V}$ and $Fc/Fc^+ = 0.625\text{ V vs Ag/Ag}^+$ in acetonitrile) by cyclic voltammetry (CV) (Figure S1 in the Supporting Information). The XY1b and MSS redox potentials in acetonitrile, when anchored on TiO₂, are reported to be $E_{1/2} = 1.08$ and 1.18 V vs NHE , respectively.⁹ As such, the calculated driving force for regenerating the dyes' radical cations after light-induced electron injection with Cu^I(dmby)₂-TFMSI is on the low side ($\Delta G_{reg} = 0.14$ and 0.24 eV for XY1b and MSS, respectively). However, many reports on copper polypyridyl complexes state that sufficient regeneration of the oxidized dye molecules, with close to unity yield at driving force potentials as low as 0.1 V , can be attained.^{37,39}

To start, a XY1b and MSS cosensitized $1 \times 1\text{ cm}^2$ DSC was assembled with 0.1 M Cu^I and 0.05 M Cu^{II} as the redox mediator in EiPS (device A) and tested under 1000 lx irradiation from an Osram T8/930 fluorescent tube (light and photon flux spectra can be found in the Supporting Information, Figure S2). To our surprise, device A, which lacks any additives especially a Lewis base, did not show any significant photocurrent or a photovoltage when it was freshly prepared; however, after 24 h of storage in the dark a better photovoltaic performance (PCE = 3.2%) was measured at 1000 lx , as evident from the corresponding IV curve shown in Figure 1 and the presented data in Table 1. Upon the addition of the *N*-methylbenzimidazole (NMBI) Lewis base to the electrolyte system, a profound and instant enhancement of the photovoltaic parameters was seen for device B, where PCE = 19.3% was attained with an optimized concentration of 0.6 M of NMBI, Figure 1 and Table 1. Device C, which constitutes in addition to the NMBI Lewis base in the Cu^I/Cu^{II} electrolyte and a 10% of the ionic liquid 1-butyl-3-methylimidazolium bis(trifluoromethylsulfonyl)imide (ImTFMSI), did not show significant enhancements in the DSC's photovoltaic parameters (PCE = 19.5%). However, upon the addition of 0.1 M LiTFMSI instead of ImTFMSI (as in device D) or in addition to the latter (as in device E), enhancements in the short-circuit currents of both devices were seen ($J_{sc} = 103$ and $107\text{ }\mu\text{A}\cdot\text{cm}^{-2}$, respectively), and consequently an increase in the DSCs' efficiencies (PCE of 22.2% and 23.3% for devices D and E, respectively). The corresponding IPCE% spectra of the five devices A–E in the range 350–750 nm and the corresponding

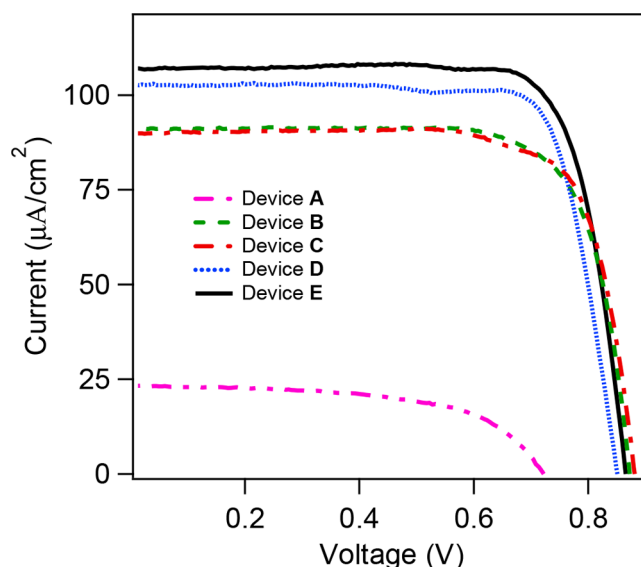


Figure 1. Photocurrent–photovoltage response (IV curves) of XY1b and MSS cosensitized $1 \times 1\text{ cm}^2$ DSCs (devices A–E) with different additives to the Cu^(I)/Cu^(II) electrolyte system in EiPS under 1000 lx fluorescent light irradiation.

integrated spectra using the photon flux of the fluorescent lamp are shown in Figure S3.

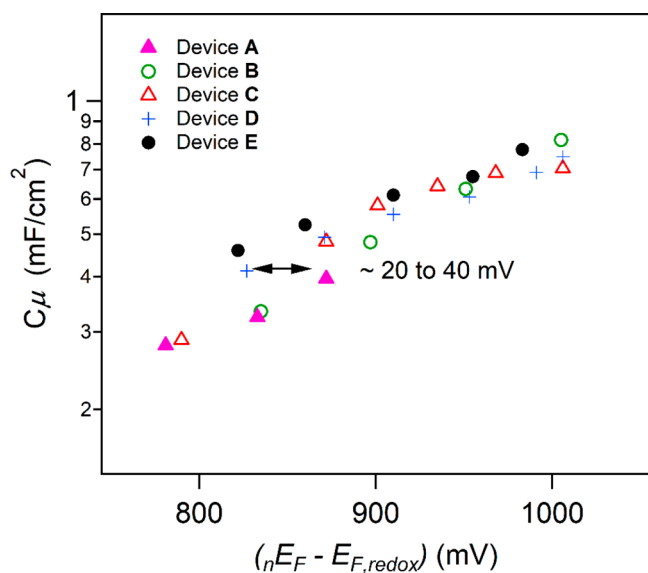
Comparing devices B and C, one can deduce that the addition of ImTFMSI to the electrolyte, which might increase both the ionic and electric conductivity, does not have a significant effect on the DSC's performance. However, the addition of LiTFMSI in devices D and E resulted in an increase in J_{sc} when compared to devices B and C. Lithium ions are well-known to lead to deeper surface states below the conduction band edge of titania (E_C) and lowering of the electron quasi-Fermi energy level in the TiO₂ film (${}_nE_F$) at a given electron injection rate, in addition to lowering of the former.^{40–42} Therefore, the decrease of the V_{OC} by $\sim 20\text{ mV}$ when comparing the two pairs of devices (device B with D and device C with E) is probably due to the narrower energy difference (${}_nE_F - E_{F,redox}$) between the titania ${}_nE_F$ and the electrolyte Fermi level ($E_{F,redox}$), while the enhancement of J_{sc} values suggests better electron injection and/or collection upon lowering the E_C in devices D and E when compared to B and C, respectively.

In order to investigate further the above-mentioned results (lowering of ${}_nE_F$ by Li⁺), we performed electrochemical impedance spectroscopy (EIS) measurements on the five different devices at V_{OC} under different light intensities (Nyquist and Bode plots are shown in Figures S5–S9). It is worth mentioning here that the EIS parameters for device A were roughly estimated due to the high resistance values measured in this device as seen in Figure S9. Figure 2 shows plots of the chemical capacitance ($C\mu$) values at the TiO₂/electrolyte interface for devices A–E. As can be seen, devices D and E, both of which contain lithium ions, show a shift $\Delta({}_nE_F - E_{F,redox})$ of ~ 20 – 40 mV lower than devices A, B, and C that lack any Li⁺ at a certain $C\mu$ value under low light intensities (below 2000 lx). A shift in the (${}_nE_F - E_{F,redox}$) toward higher or lower values is usually attributed to an upward or downward shift in ${}_nE_F$ with respect to the electrolyte $E_{F,redox}$ respectively. In this context, the addition of cation additives leads to a downward shift in the ${}_nE_F$ and hence to an

Table 1. Photovoltaic Parameters of the Different $1 \times 1 \text{ cm}^2$ DSC Devices under 1000 lx ($311 \mu\text{W}\cdot\text{cm}^{-2}$) Light Irradiation

device	electrolyte	J_{sc} ($\mu\text{A}\cdot\text{cm}^{-2}$)	V_{oc} (mV)	FF	power out ($\mu\text{W}\cdot\text{cm}^{-2}$)	PCE (%) ^d
A ^a	0.1 M Cu ^I and 0.05 M Cu ^{II}	23 ± 5 (29) ^c	724	0.59	9.9	3.2
B	0.1 M Cu ^I , 0.05 M Cu ^{II} , and 0.6 M NMBI	91 ± 3 (89) ^c	874	0.75	60.1	19.3
C ^b	0.1 M Cu ^I , 0.05 M Cu ^{II} , 0.6 M NMBI, and 10% IL	90 ± 3 (90) ^c	882	0.77	60.8	19.5
D	0.1 M Cu ^I , 0.05 M Cu ^{II} , 0.6 M NMBI, and 0.1 M LiTFMSI	103 ± 2 (97) ^c	852	0.79	68.9	22.2
E ^b	0.1 M Cu ^I , 0.05 M Cu ^{II} , 0.6 M NMBI, 0.1 M LiTFMSI, and 10% IL	107 ± 2 (102) ^c	866	0.78	72.5	23.3

^aThe presented data were measured after 24 h of storage in the dark. ^bThe 10% ionic liquid (IL), 1-butyl-3-methylimidazolium bis(trifluoromethylsulfonyl)imide, used corresponds to $\sim 0.34 \text{ M}$ at 20°C . ^cIntegrated photocurrent (at 1000 lx). ^dDyes' loadings were measured to be ~ 9.0 and $3.0 \times 10^{-8} \text{ mol}\cdot\text{cm}^{-2}$ for XY1b and MSS in all of the devices, respectively.

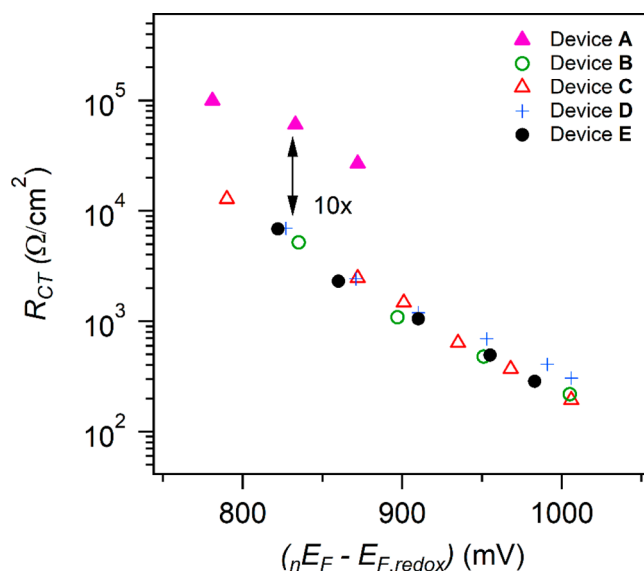
**Figure 2.** Chemical capacitance (C_μ) values at the TiO_2 /electrolyte interface for devices A–E.

increase in J_{sc} and a decrease in V_{OC} .^{43,44} In addition, we performed Mott–Schottky experiments on five undyed devices using the same electrolyte compositions as those in the DSCs of A–E, Figure S4. The Mott–Schottky plots of the undyed devices resonate with the EIS experiments performed on the dye-sensitized devices A–E, where a downward shift in the titania flat-band potential is seen upon the addition of Li^+ in the electrolyte composition (as in the electrolytes of devices D and E). Therefore, the lower V_{OC} values observed in devices D and E, as compared to the others, could be attributed to the titania nE_F downward shift resulting from the addition of Li^+ .

Interestingly, devices A, B, and C have very similar C_μ values at the same V_{OC} values, suggesting that ImTFMSI, and unlike Li^+ , has no profound effects on the titania/electrolyte interface most probably due to the inability of the larger Im⁺ to intercalate into the titania film. An additional insight derived from Figure 2 is the negligible influence of NMBI in our EiPS-based medium on the titania nE_F , while conventionally the base is known to cause an upward shift in the nE_F (devices B and C vs A).

A similar finding that aligns with our observation was reported by Yamamoto et al.³² in the iodine/iodide electrolyte system in EiPS and was attributed to the fact that EiPS has a high donor number (DN ~ 16.1) that trounces the effect of NMBI in a DSC. This indicates that in our EiPS-based medium, NMBI has minimal impact on the nE_F . However, the absence of NMBI appears to have a profound positive effect on the R_{CT} values at the TiO_2 /electrolyte interface. In particular,

Figure 3 depicts that device A (aged for 24 h) showed a significantly higher R_{CT} , approximately 10 times greater than

**Figure 3.** Charge transfer resistance (R_{CT}) values at the TiO_2 /electrolyte interface for devices A–E.

the other devices, suggesting a slower charge recombination. This latter finding is consistent with the dark currents measured for devices A when compared to device B, where the former shows lower dark currents than that of the latter at the same voltage values, Figure 4. Additionally, a recent study by Bach et al. showed the importance of coordination of strong Lewis bases such as 4-*tert*-butylpyridine (TBP) and NMBI with $\text{Cu}^{(II)}$ phenanthroline complexes for better performance of such copper electrolytes in DSCs.⁴⁵ It was shown that the coordination of the Lewis base to the $\text{Cu}(\text{II})$ center efficiently slows down recombination; however, this is not the case in our system. Based on these findings, we can infer from the EIS experiments and the dark current IV curves that the introduction of NMBI not only improves the performance of the DSC but also accelerates its electron recombination processes, as observed in devices B–E. As such, while the EIS experiments provided valuable insights about the differences in performance of the different devices, they failed to offer a satisfactory explanation for the poor photovoltaics parameters measured for device A (fresh or aged) when compared to the four devices. Therefore, we decided to explore alternative characterization techniques to gain a deeper understanding of the mechanisms at play in our system.

In order to make sure that the low performance of device A (fresh or aged for 24 h) is not due to poor dye regeneration

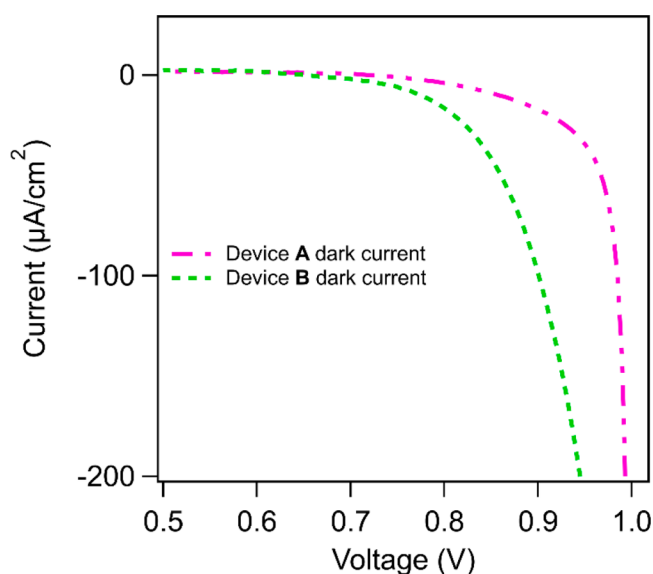


Figure 4. Dark currents measured for devices A and B.

efficiency by the electrolyte system that lacks NMBI, photoinduced absorption spectroscopy (PIA)⁴⁶ experiments were performed on cosensitized XY1b/MSS titania films with and without either NMBI and Cu^{I/II} or both in EiPS, Figure 5

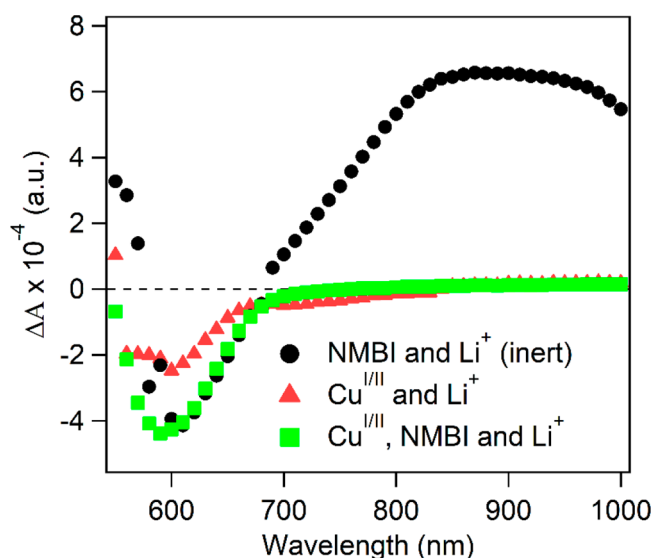


Figure 5. PIA spectra of cosensitized XY1b/MSS titania films with and without either NMBI and Cu^{I/II} or both in EiPS.

(PIA spectra of individually sensitized DSCs data can be found in Figure S10). Figure 5 clearly demonstrates that in the absence of the copper electrolyte, the PIA spectrum of the cosensitized TiO₂ film (denoted as inert) exhibits a bleach at approximately 600 nm. This latter is attributed to the ground-state bleach of the dyes upon their oxidation and to the Stark shift effect.^{47,48} One can also observe a wide absorption peak between 670 and 1000 nm corresponding to the oxidized dyes (dye^{•+}). However, the latter absorption feature disappears in the presence of the copper electrolyte, irrespective of the presence or absence of NMBI (when freshly prepared or when aged), suggesting an efficient regeneration of the oxidized dyes by the different electrolyte compositions. The same finding was

also evident in the individually sensitized XY1b and MSS titania in the presence of the copper electrolyte, Figure S10. Therefore, the low performance of device A (fresh or aged) does not seem to be due to inefficient regeneration of the dye^{•+} with the Cu^I complex. In addition, the fact that we did not see higher recombination processes in device A when compared to device B in the previously mentioned EIS data (such as between the injected electrons in titania to the dye^{•+} in the case of inefficient dye regeneration) supports the PIA findings.

Nevertheless, the above findings do not negate the assumption that the dyes' regeneration kinetics might be faster in device B when compared to A. This is supported by the observation that the addition of NMBI results in a shift in the E_{ox} to lower values; thus higher ΔG_{reg} has been found in our system. These findings are consistent with the results seen by Bach et al. with a similar Cu^{II} complex of 2,9-dimethyl-1,10-phenanthroline.⁴⁵ Figure 6 shows the cyclic voltammograms

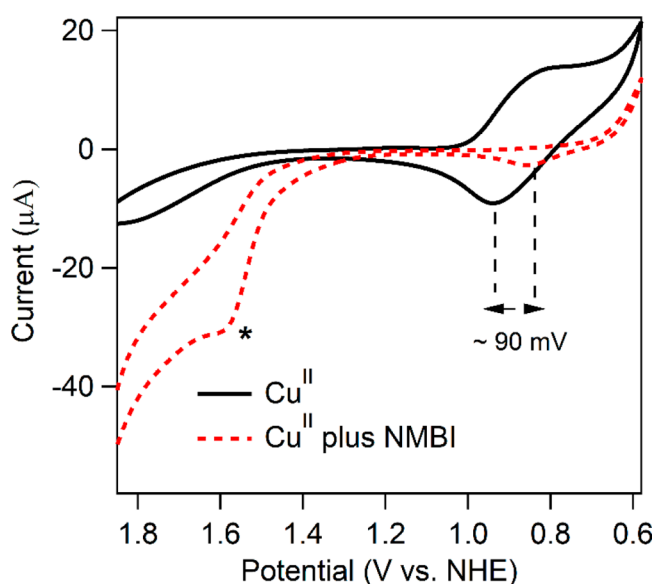


Figure 6. Cyclic voltammograms of the Cu^{II} complex in the presence and absence of NMBI measured in acetonitrile at a scan rate of 100 mV·s⁻¹ with a platinum working electrode. The irreversible oxidation peak of NMBI is denoted by an asterisk.

(CV) of the Cu^{II} complex, where a shift of around 90 mV to a lower potential is seen in the oxidation peak of the complex upon the addition of NMBI in acetonitrile. The shift in the E_{ox} of the Cu^{II} complex in the presence of NMBI is most probably due to the well-known coordination of Lewis bases to the Cu^{II} but not Cu^I metal centers.^{45,49}

At this stage, it appears that the major influence of the NMBI in the redox electrolyte system on the performance of the DSCs is not primarily occurring at the titania-dye/electrolyte interface. Thus, in order to complete the picture, dummy cells incorporating the Cu^I and Cu^{II} complexes in the presence and absence of NMBI (CE/electrolyte/CE) were assembled using PEDOT CEs. Tafel plots and EIS experiments were performed in order to assess the regeneration of the Cu^{II} species in the DSCs at the counter electrode (CE). Figure 7 presents the Tafel plots of two dummy cells A' (with fresh electrolyte and after aging for 24 h) and B'. The dummy cell A' containing a freshly prepared electrolyte (lacking NMBI) shows two Tafel regions that we speculate is due to the presence of two different Cu^{II} species, each displaying very

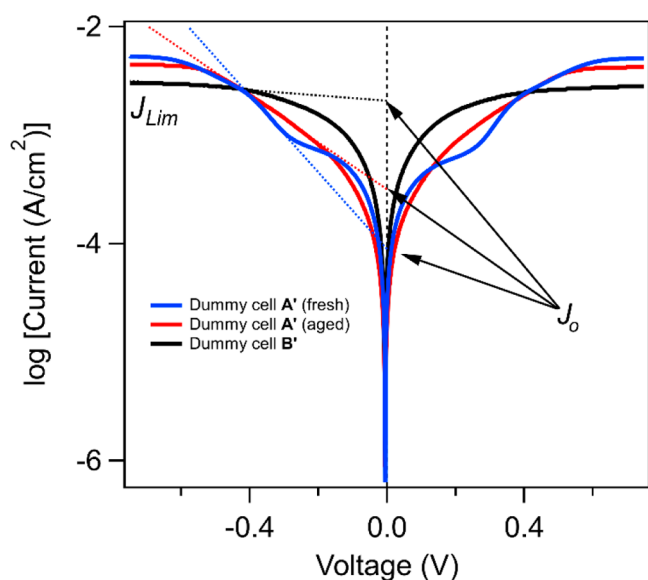


Figure 7. Tafel plots for the fresh and aged dummy cells A' and dummy cell B'.

different electroactivity at the CE. Interestingly, after 1 day, as can be seen for the aged dummy cell A', the Tafel polarization spectrum shows one dominant Tafel region. As for the dummy cell B', it gave rise to one Tafel region in the Tafel polarization spectrum, which stabilizes within 1 h and remains unchanged for up to 4 days. The exchange current densities values (J_0) of the fresh and aged dummy cell A' and that of B' were evaluated to be $J_0 = 0.09$ and ~ 0.3 (fresh dummy cell A'), 0.32 (aged dummy cell A'), and $2.08 \text{ mA}\cdot\text{cm}^{-2}$ (dummy cell B'). In fact, to evaluate the quality of DSCs, the J_0 values can be used to approximate the short-circuit photocurrent (J_{sc}) densities observed under high light illumination (such as 1 sun). Figure S11 and Table S1 depict the IV curves and photovoltaic parameters, respectively, for devices A–E measured under simulated AM 1.5G solar light irradiation ($100 \text{ mW}\cdot\text{cm}^{-2}$). Indeed the above-mentioned correlation was present in our case, as the J_0 values for dummy cells A' (aged) and B' were comparable to the J_{sc} densities of devices A and B–E under 1 sun irradiation ($J_{sc} \sim 0.5$ and $1.5 \text{ mA}\cdot\text{cm}^{-2}$, respectively), Figure S11 and Table S1. Additionally, the value of J_0 is a kinetic component directly correlated with the electrochemical reaction that is inversely proportional to R_{CT} , as described in eq 1.

$$J_0 = \frac{RT}{nFR_{CT}} \quad (1)$$

where R is the gas constant, T is the absolute temperature, n is the number of electrons associated with reaction, and F is the Faraday constant. Applying eq 1, the calculated R_{CT} for the fresh and aged dummy cell A' and that of B' are R_{CT} (from Tafel) = 288 and ~ 80 (fresh dummy cell A'), 81 (aged dummy cell A'), and $12 \text{ }\Omega\cdot\text{cm}^2$ (dummy cell B'). It is important to mention here that the two observed J_0 values and the two R_{CT} values for the fresh dummy cell A' correspond to the presence of two supposedly distinct Tafel regions, indicating the existence of two different Cu species. Further investigation will be conducted to provide evidence supporting this claim.

In addition, the diffusion coefficients of the Cu^{II} species present in the EiPS based dummy cells A' (aged) and B' were

calculated to be $D_{\text{Cu}^{\text{II}}} = 1.2 \times 10^{-6}$ and $7.8 \times 10^{-7} \text{ cm}^2\cdot\text{s}^{-1}$, respectively, using eq 2.

$$D = \frac{dJ_{\text{lim}}}{2nFC} \quad (2)$$

where $d = 25 \text{ }\mu\text{m}$ is the spacer thickness between the two electrodes, J_{lim} is the cathodic limiting current, $n = 1$ is the number of electrons involved in the reduction process at the electrode, F is Faraday's constant, and $C = 0.05 \text{ mM}$ is the molar concentration of the limiting species Cu^{II} in the electrolyte. As pointed out before, the higher viscosity of EiPS compared to acetonitrile (ACN) is not a detriment in our case due to the low light irradiation levels used in this study rather than the standard 1 sun irradiation. Therefore, when comparing our obtained $D_{\text{Cu}^{\text{II}}}$ values in EiPS ($D_{\text{Cu}^{\text{II}}} = 1.2 \times 10^{-6}$ and $7.8 \times 10^{-7} \text{ cm}^2\cdot\text{s}^{-1}$ in aged dummy cell A' and dummy cell B', respectively) to the values reported in the literature for the same complex, $\text{Cu}^{\text{II}}(\text{dmby})\text{TFMSI}/\text{Cl}$ in acetonitrile (ACN) ($D_{\text{Cu}^{\text{II}}} = 3.3 \times 10^{-5} \text{ cm}^2\cdot\text{s}^{-1}$),³⁷ it is evident that our values are smaller than those in ACN. Interestingly, this difference did not negatively affect the photovoltaic parameters of the five devices (A–E) when measured at 1000 lx. However, it is important to note that the situation changes when we work under 1 sun irradiation conditions, where the considerably low $D_{\text{Cu}^{\text{II}}}$ values mentioned above have a more pronounced effect in our system. In other words, as shown in Figure S11, the obtained J_{sc} values for devices A and B in EiPS are approximately 0.5 and $1.5 \text{ mA}\cdot\text{cm}^{-2}$, respectively, under 1 sun irradiation, while in ACN based DSCs J_{sc} values are typically higher (between 12 and $16 \text{ mA}\cdot\text{cm}^{-2}$) under similar conditions.^{9,37,39} This can be attributed to the higher viscosity of the EiPS solvent compared to that of ACN that leads to more profound mass transfer issues at high light intensities. Based on these results and comparisons, we can generalize that despite the low $D_{\text{Cu}^{\text{II}}}$ values in our EiPS electrolyte medium, which are often associated with low efficiency DSCs, this is not detrimental under low light conditions.

Additionally, R_{CT} values can be obtained from the EIS Nyquist plots performed on the dummy cells, along with the $C\mu$ values, as shown in Figure 8. These plots were recorded at 0 V for the fresh and aged dummy cells A', as well as for dummy cell B'. However, we encountered difficulties in accurately fitting the EIS data of the fresh dummy cells A' most probably due to the presence of two electroactive Cu^{II} species with different electroactivities at the CE. On the other hand, for the aged dummy cell A' and dummy cell B', we successfully extracted the R_{CT} – $C\mu$ values at the CE/electrolyte interface from the fitted data using the equivalent circuit shown in the inset of Figure 8. These values were R_{CT} (from EIS) = 75.5 and $8.9 \text{ }\Omega\cdot\text{cm}^2$ and $C\mu = 0.66$ and $1.20 \text{ mF}\cdot\text{cm}^{-2}$ for the aged dummy cell A' and dummy cell B', respectively. Hence, the smaller R_{CT} of the dummy cell B' compared to that of A' (measured by EIS and/or derived from the Tafel plots to be 8.9 – 12 vs ~ 75.5 – $81 \text{ }\Omega\cdot\text{cm}^2$, respectively) suggests a higher electrocatalytic activity of the PEDOT-CE on the Cu^{II} species within the dummy cell B'.

Based on the results obtained from the Tafel and EIS experiments, we propose that in our medium, the Cu^{II} species in the presence of NMBI (such as in devices B–E and dummy cell B') most likely exists as a highly coordinated complex with a 5 or 6 coordinated metal center. The suggested complex has the form $\text{Cu}^{\text{II}}(\text{dmby})_2(\text{NMBI})_{1/2}^{+2}$, where NMBI acts as a coordinating ligand. This highly coordinated complex exhibits

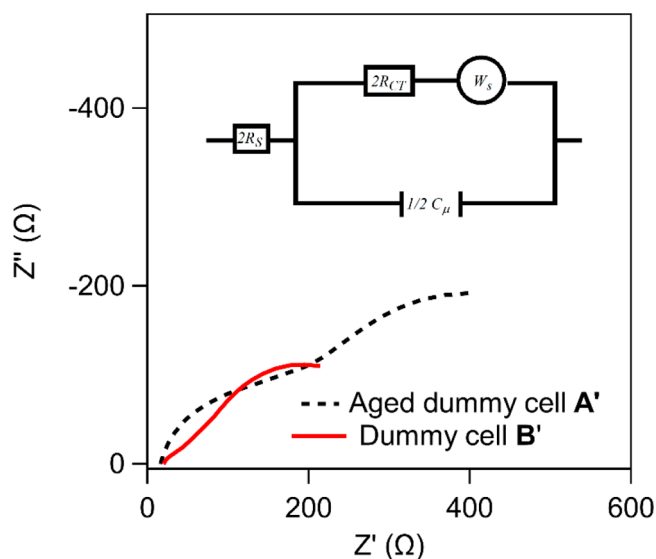


Figure 8. Nyquist plots recorded at 0 V for the aged dummy cell A' and dummy cell B'.

a high electrocatalytic activity at the PEDOT-CE, as indicated by the lower R_{CT} values from the Tafel and EIS experiments for dummy cell B'. This electrocatalytic activity might be one of the reasons behind the improved performance of the devices containing NMBI (devices B–E). However, when NMBI is absent, as in device A and aged dummy cell A', the medium only contains our copper redox mediators in our EiPS solvent. In this case, the Cu^{II} complex is most likely in the form $\text{Cu}^{\text{II}}(\text{dmby})_2\text{S}_{1/2}^{+2}$, where S represents the solvent EiPS. This complex exhibits higher R_{CT} values in aged dummy cell A' compared to dummy cell B', indicating a lower electrocatalytic activity at the PEDOT-CE. This explains the poor performance of device A. Furthermore, in the case of the fresh dummy cell A', the Cu^{II} center may be in the form $\text{Cu}^{\text{II}}(\text{dmby})_2\text{X}_{1/2}^{+/0}$ and $\text{Cu}^{\text{II}}(\text{dmby})_2\text{S}_{1/2}^{+2}$, where X^- represents a chloride and/or TFMSI⁻ anion that could be labile in coordinating solvents such as EiPS. This suggests the possibility of having two different species in the fresh dummy cell A'. Upon aging, EiPS fully coordinates instead of X^- , resulting in a single species, most likely $\text{Cu}^{\text{II}}(\text{dmby})_2\text{S}_{1/2}^{+2}$ observed in aged dummy cell A'.

To further support our suggested theory, we conducted UV–vis experiments to investigate the effect of adding NMBI and EiPS to our Cu^{II} complex. Our aim was to confirm whether these species would coordinate as ligands and form new complexes. In order to ensure accuracy, the experiment was performed in a noncoordinating solvent, dichloromethane. Figure 9 illustrates the spectra recorded for the Cu^{II} complexes in the absence and presence of either NMBI or EiPS in dichloromethane. As depicted in Figure 9, an instant change of the Cu^{II} spectrum resulted upon the addition of 30 equiv of NMBI with a ~ 58 nm blue-shift of the 730 nm band and a concurrent enhanced absorption of the 453 nm, whereas upon the addition of 5% in volume of EiPS to the Cu^{II} a very slow change in the spectrum was observed, where a constant enhanced absorption at 453 nm was seen over the course of a couple of days with a concurrent small decrease in the 730 nm band. No change in the Cu^{I} complex spectrum was seen upon the addition of NMBI nor EiPS, Figure S12.

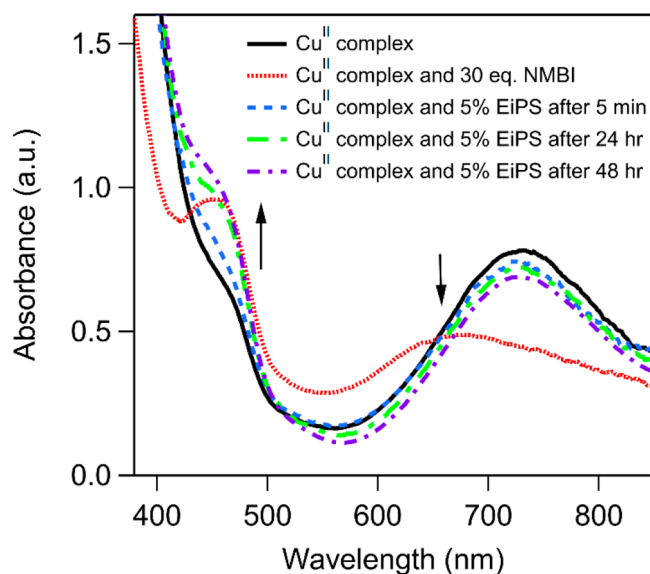


Figure 9. UV–vis experiments for the Cu^{II} complex in the presence of either NMBI or EiPS in dichloromethane.

To conclude, the obtained results clearly demonstrate that EiPS acts as a weak coordinating ligand, where its coordination reaction with $\text{Cu}^{\text{II}}(\text{dmby})_2\text{X}_{1/2}^{+/0}$ is comparatively slow. This phenomenon provides an explanation for the presence of two distinct Tafel regions in the Tafel plots of the fresh dummy cell A', which eventually gives rise to a single region as it ages. In addition, this slow ligand substitution reaction explains why device A shows better photovoltaic performance after 24 h of its assembly with a freshly prepared electrolyte. In contrast, NMBI coordinates more rapidly to the Cu^{II} species upon introduction into the electrolyte. This explains why the Tafel polarization spectrum of dummy cell B' stabilizes almost within an hour and remains unchanged afterward. The proposed ligand substitution reactions are shown in Scheme 1.

To assess the long-term stability of the EiPS based DSCs, devices B–E were subjected to light soaking of 10 klx irradiation from a white LED for 1270 h. Currently, there are no established standards for conducting long-term stability testing of indoor DSCs. However, in our study, we opted for a higher illumination intensity than the reported range in the literature, which falls between 200 and 6000 lx.^{13,17–22} Figure 10 shows the evolution of the average photovoltaic parameters measured at 1000 lx of the four different devices. As can be seen, the photovoltaic parameters of device B stayed somehow constant over the course of the long-term testing retaining 97% of the initial PCE% after 53 days of constant 10 klx irradiation (initial and final PCE% = 19.3 and 18.7%, respectively), while devices C–E started to fail around 38, 25 and less than 18 days, respectively. Closely inspecting the sealed devices C–E at the point when they started to fail, precipitates of the copper complexes were observed in the electrolyte (Figure S13), unlike device B which did not show such a phenomenon. We speculate that the presence of either LiTFMSI, the IL ImTFMSI, or both in the electrolytes of devices C, D, and E, respectively, causes precipitation of the Cu^{II} electrolyte component after prolonged time most probably due to a salting out effect. Additionally, we investigated the desorption of the dyes from a $1 \times 1 \text{ cm}^2$ XY1b/MS5 cosensitized titania film versus time in 10 mL EiPS, Figure S14. As can be seen, a substantial desorption ($\sim 70\%$) of the dyes was measured over

Scheme 1. Proposed Ligand Substitution Reactions, Where S Represents the Solvent EiSP and X⁻ Either TFMSI⁻ or Cl⁻

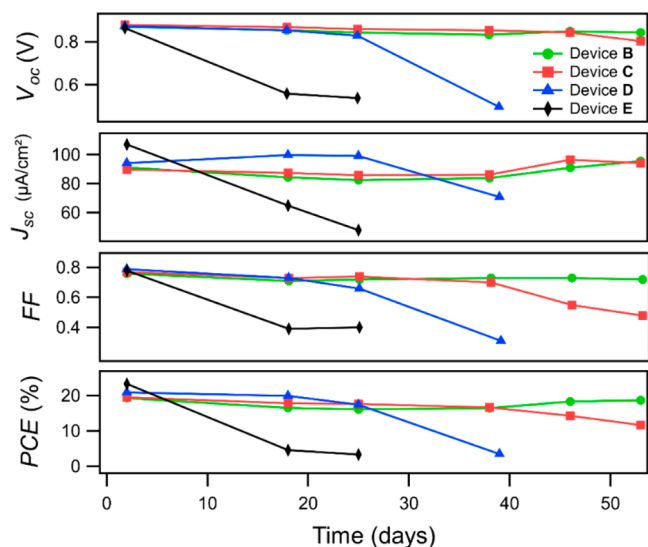
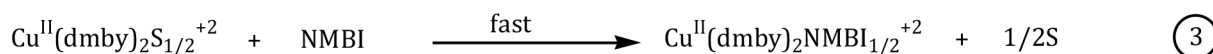
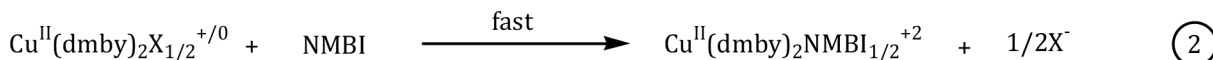
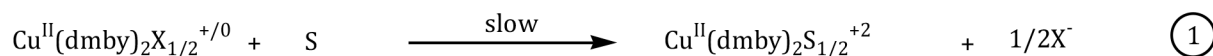


Figure 10. Performance of devices B–E at 1000 lx after 10 klx light soaking for 53 days.

the course of 1 week; however, this was not detected by the naked eye in our devices during the long-term stability experiments. We attribute the latter finding to the fact that the used electrolyte volume in any of the assembled DSCs is approximately 3–5 μL , which is too small, when compared to a volume of 10 mL, to cause profound desorption of the dyes. However, this does not negate the fact that some dye(s) desorption might take place over time.

CONCLUSION

In summary, we have successfully fabricated a long-term stable DSC using the high boiling point, low vapor pressure solvent, EiPS, that incorporates a copper-based redox mediator in conjunction with the XY1b and MS5 dyes. It was demonstrated that to achieve both optimal performance and stability of the DSC in the newly tested electrolyte medium, specific electrolyte compositions should be employed. In other words, device B, which solely contained NMBI, demonstrated the most favorable long-term stability among the tested devices, a PCE of 19.3%. This outcome was attributed to the essential role of the NMBI Lewis base, which rapidly coordinates as a fifth/sixth ligand and hence improves the device's R_{CT} at the electrolyte/CE interface, leading to this high PCE. However, devices C–E that contained Li⁺ and/or IL exhibited the highest PCEs among all the tested devices. Unfortunately, they displayed inadequate long-term stability and began to deteriorate at around days 38, 25, and less than 18, respectively. This deterioration is likely caused by the precipitation of Cu^{II} complex(es) in the electrolyte, which were

observed visually. Therefore, device B exhibited the best compromise between a high efficiency and durable stability.

ASSOCIATED CONTENT

Supporting Information

The Supporting Information is available free of charge at <https://pubs.acs.org/doi/10.1021/acsaem.3c02067>.

Further EIS and CV measurements, IV curves, and IPCE % spectra under 1 sun irradiation, in addition to the light spectrum (PDF)

AUTHOR INFORMATION

Corresponding Author

Tarek H. Ghaddar – Department of Chemistry, American University of Beirut, Beirut 11-0236, Lebanon; orcid.org/0000-0002-7748-0597; Phone: +961-1-350000 (ext 4057); Email: tarek.ghaddar@aub.edu.lb; Fax: +961-1-365217

Author

Daniela Sayah – Department of Chemistry, American University of Beirut, Beirut 11-0236, Lebanon

Complete contact information is available at: <https://pubs.acs.org/10.1021/acsaem.3c02067>

Notes

The authors declare no competing financial interest.

ACKNOWLEDGMENTS

This work was supported by the University Research Board (Grant 2629S) at the American University of Beirut (AUB) and the Munib and Angela Masri Institute of Energy and Natural Resources (Grant 26709).

REFERENCES

- O'Regan, B.; Grätzel, M. A low-cost, high-efficiency solar cell based on dye-sensitized colloidal TiO₂ films. *Nature* **1991**, 353 (6346), 737–740.
- Sharmoukh, W.; Cong, J.; Ali, B. A.; Allam, N. K.; Kloo, L. Comparison between Benzothiadiazole–Thiophene- and Benzothiadiazole–Furan-Based D–A– π –A Dyes Applied in Dye-Sensitized Solar Cells: Experimental and Theoretical Insights. *ACS Omega* **2020**, 5 (27), 16856–16864.
- Sharmoukh, W.; Cong, J.; Gao, J.; Liu, P.; Daniel, Q.; Kloo, L. Molecular Engineering of D–D– π –A-Based Organic Sensitizers for Enhanced Dye-Sensitized Solar Cell Performance. *ACS Omega* **2018**, 3 (4), 3819–3829.
- Ellis, H.; Vlachopoulos, N.; Häggman, L.; Perruchot, C.; Jouini, M.; Boschloo, G.; Hagfeldt, A. PEDOT counter electrodes for dye-sensitized solar cells prepared by aqueous micellar electrodeposition. *Electrochim. Acta* **2013**, 107, 45–51.
- Suresh, S.; Unni, G. E.; Satyanarayana, M.; Nair, A. S.; Pillai, V. M. Silver nanoparticles-incorporated Nb₂O₅ surface passivation layer

for efficiency enhancement in dye-sensitized solar cells. *J. Colloid Interface Sci.* **2018**, *524*, 236–244.

(6) Masud; Kim, H. K. Redox Shuttle-Based Electrolytes for Dye-Sensitized Solar Cells: Comprehensive Guidance, Recent Progress, and Future Perspective. *ACS omega* **2023**, *8* (7), 6139–6163.

(7) Muñoz-García, A. B.; Benesperi, I.; Boschloo, G.; Concepcion, J. J.; Delcamp, J. H.; Gibson, E. A.; Meyer, G. J.; Pavone, M.; Pettersson, H.; Hagfeldt, A.; Freitag, M. Dye-sensitized solar cells strike back. *Chem. Soc. Rev.* **2021**, *50* (22), 12450–12550.

(8) Aftabzaman, M.; Sarker, S.; Lu, C.; Kim, H. K. In-depth understanding of the energy loss and efficiency limit of dye-sensitized solar cells under outdoor and indoor conditions. *Journal of Materials Chemistry A* **2021**, *9* (44), 24830–24848.

(9) Zhang, D.; Stojanovic, M.; Ren, Y.; Cao, Y.; Eickemeyer, F. T.; Socie, E.; Vlachopoulos, N.; Moser, J.-E.; Zakeeruddin, S. M.; Hagfeldt, A.; Grätzel, M. A molecular photosensitizer achieves a Voc of 1.24 V enabling highly efficient and stable dye-sensitized solar cells with copper(II/I)-based electrolyte. *Nat. Commun.* **2021**, *12* (1), 1777.

(10) Hora, C.; Santos, F.; Sales, M. G. F.; Ivanou, D.; Mendes, A. Dye-Sensitized Solar Cells for Efficient Solar and Artificial Light Conversion. *ACS Sustainable Chem. Eng.* **2019**, *7* (15), 13464–13470.

(11) Haridas, R.; Velore, J.; Pradhan, S. C.; Vindhyasarumi, A.; Yoosaf, K.; Soman, S.; Unni, K. N. N.; Ajayagosh, A. Indoor light-harvesting dye-sensitized solar cells surpassing 30% efficiency without co-sensitizers. *Materials Advances* **2021**, *2* (23), 7773–7787.

(12) Liu, I. P.; Lin, W.-H.; Tseng-Shan, C.-M.; Lee, Y.-L. Importance of Compact Blocking Layers to the Performance of Dye-Sensitized Solar Cells under Ambient Light Conditions. *ACS Appl. Mater. Interfaces* **2018**, *10* (45), 38900–38905.

(13) Venkatesan, S.; Lin, W.-H.; Teng, H.; Lee, Y.-L. High-Efficiency Bifacial Dye-Sensitized Solar Cells for Application under Indoor Light Conditions. *ACS Appl. Mater. Interfaces* **2019**, *11* (45), 42780–42789.

(14) Cao, Y.; Liu, Y.; Zakeeruddin, S. M.; Hagfeldt, A.; Grätzel, M. Direct Contact of Selective Charge Extraction Layers Enables High-Efficiency Molecular Photovoltaics. *Joule* **2018**, *2* (6), 1108–1117.

(15) Michaels, H.; Rinderle, M.; Freitag, R.; Benesperi, I.; Edvinsson, T.; Socher, R.; Gagliardi, A.; Freitag, M. Dye-sensitized solar cells under ambient light powering machine learning: towards autonomous smart sensors for the internet of things. *Chem. Sci.* **2020**, *11* (11), 2895–2906.

(16) Michaels, H.; Rinderle, M.; Benesperi, I.; Freitag, R.; Gagliardi, A.; Freitag, M. Emerging indoor photovoltaics for self-powered and self-aware IoT towards sustainable energy management. *Chemical Science* **2023**, *14* (20), 5350–5360.

(17) Venkatesan, S.; Hsu, T.-H.; Teng, H.; Lee, Y.-L. Dye-Sensitized Solar Cells with Efficiency over 36% under Ambient Light Achieved by Cosensitized Tandem Structure. *Solar RRL* **2023**, *7* (11), 2300220.

(18) Juang, S. S.; Lin, P. Y.; Lin, Y. C.; Chen, Y. S.; Shen, P. S.; Guo, Y. L.; Wu, Y. C.; Chen, P. Energy Harvesting Under Dim-Light Condition With Dye-Sensitized and Perovskite Solar Cells. *Front. Chem.* **2019**, *7*, 209.

(19) Venkatesan, S.; Liu, I. P.; Li, C.-W.; Tseng-Shan, C.-M.; Lee, Y.-L. Quasi-Solid-State Dye-Sensitized Solar Cells for Efficient and Stable Power Generation under Room Light Conditions. *ACS Sustainable Chem. Eng.* **2019**, *7* (7), 7403–7411.

(20) Wang, C.-L.; Lin, P.-T.; Wang, Y.-F.; Chang, C.-W.; Lin, B.-Z.; Kuo, H.-H.; Hsu, C.-W.; Tu, S.-H.; Lin, C.-Y. Cost-effective anthryl dyes for dye-sensitized cells under one sun and dim light. *J. Phys. Chem. C* **2015**, *119* (43), 24282–24289.

(21) Chou, H.-H.; Liu, Y.-C.; Fang, G.; Cao, Q.-K.; Wei, T.-C.; Yeh, C.-Y. Structurally simple and easily accessible perylenes for dye-sensitized solar cells applicable to both 1 sun and dim-light environments. *ACS Appl. Mater. Interfaces* **2017**, *9* (43), 37786–37796.

(22) Santos, F.; Martins, J.; Capitão, J.; Emami, S.; Ivanou, D.; Mendes, A. Stable Cobalt-Mediated Monolithic Dye-Sensitized Solar Cells by Full Glass Encapsulation. *ACS Applied Energy Materials* **2022**, *5* (6), 7220–7229.

(23) Venkatesan, S.; Hsu, T.-H.; Wong, X.-W.; Teng, H.; Lee, Y.-L. Tandem dye-sensitized solar cells with efficiencies surpassing 33% under dim-light conditions. *Chemical Engineering Journal* **2022**, *446*, 137349.

(24) Venkatesan, S.; Lin, W.-H.; Hsu, T.-H.; Teng, H.; Lee, Y.-L. Indoor Dye-Sensitized Solar Cells with Efficiencies Surpassing 26% Using Polymeric Counter Electrodes. *ACS Sustainable Chem. Eng.* **2022**, *10* (7), 2473–2483.

(25) Ren, Y.; Zhang, D.; Suo, J.; Cao, Y.; Eickemeyer, F. T.; Vlachopoulos, N.; Zakeeruddin, S. M.; Hagfeldt, A.; Grätzel, M. Hydroxamic acid pre-adsorption raises the efficiency of cosensitized solar cells. *Nature* **2023**, *613* (7942), 60–65.

(26) Sauvage, F. A Review on Current Status of Stability and Knowledge on Liquid Electrolyte-Based Dye-Sensitized Solar Cells. *Adv. Chem.* **2014**, *2014*, 939525.

(27) Chen, C.-L.; Chang, T.-W.; Teng, H.; Wu, C.-G.; Chen, C.-Y.; Yang, Y.-M.; Lee, Y.-L. Highly efficient gel-state dye-sensitized solar cells prepared using poly(acrylonitrile-co-vinyl acetate) based polymer electrolytes. *Phys. Chem. Chem. Phys.* **2013**, *15* (10), 3640–3645.

(28) Liu, I. P.; Cho, Y.-S.; Teng, H.; Lee, Y.-L. Quasi-solid-state dye-sensitized indoor photovoltaics with efficiencies exceeding 25%. *Journal of Materials Chemistry A* **2020**, *8* (42), 22423–22433.

(29) Masud; Kim, K. M.; Kim, H. K. Polymer Gel Electrolytes Based on PEG-Functionalized ABA Triblock Copolymers for Quasi-Solid-State Dye-Sensitized Solar Cells: Molecular Engineering and Key Factors. *ACS Appl. Mater. Interfaces* **2020**, *12* (37), 42067–42080.

(30) Masud; Zhou, H.; Kim, H. K. Effective redox shuttles for polymer gel electrolytes-based quasi-solid-state dye-sensitized solar cells in outdoor and indoor applications: Comprehensive comparison and guidelines. *Materials Today. Energy* **2023**, *34*, 101299.

(31) Pang, H.-W.; Yu, H.-F.; Huang, Y.-J.; Li, C.-T.; Ho, K.-C. Electrospun membranes of imidazole-grafted PVDF-HFP polymeric ionic liquids for highly efficient quasi-solid-state dye-sensitized solar cells. *Journal of Materials Chemistry A* **2018**, *6* (29), 14215–14223.

(32) Yanada, K.; Chiba, K.; Yamaguchi, Y.; Yamamoto, H. Characteristics of Dye-sensitized Solar Cells using Linear Sulfones as an Electrolyte Solvent. *Electrochemistry* **2011**, *79* (3), 163–167.

(33) Perganti, D.; Kontos, A. G.; Stergiopoulos, T.; Likodimos, V.; Farnell, J.; Milliken, D.; Desilvestro, H.; Falaras, P. Thermal Stressing of Dye Sensitized Solar Cells Employing Robust Redox Electrolytes. *Electrochim. Acta* **2015**, *179*, 241–249.

(34) Marszalek, M.; Arendse, F. D.; Decoppet, J.-D.; Babkair, S. S.; Ansari, A. A.; Habib, S. S.; Wang, M.; Zakeeruddin, S. M.; Grätzel, M. Ionic Liquid–Sulfolane Composite Electrolytes for High-Performance and Stable Dye-Sensitized Solar Cells. *Adv. Energy Mater.* **2014**, *4* (6), 1301235.

(35) Wang, P.; Yang, L.; Wu, H.; Cao, Y.; Zhang, J.; Xu, N.; Chen, S.; Decoppet, J.-D.; Zakeeruddin, S. M.; Grätzel, M. Stable and Efficient Organic Dye-Sensitized Solar Cell Based on Ionic Liquid Electrolyte. *Joule* **2018**, *2* (10), 2145–2153.

(36) Michaels, H.; Benesperi, I.; Freitag, M. Challenges and prospects of ambient hybrid solar cell applications. *Chemical Science* **2021**, *12* (14), 5002–5015.

(37) Saygili, Y.; Söderberg, M.; Pellet, N.; Giordano, F.; Cao, Y.; Muñoz-García, A. B.; Zakeeruddin, S. M.; Vlachopoulos, N.; Pavone, M.; Boschloo, G.; Kavan, L.; Moser, J.-E.; Grätzel, M.; Hagfeldt, A.; Freitag, M. Copper Bipyridyl Redox Mediators for Dye-Sensitized Solar Cells with High Photovoltage. *J. Am. Chem. Soc.* **2016**, *138* (45), 15087–15096.

(38) Chiba, K.; Ueda, T.; Yamaguchi, Y.; Oki, Y.; Shimodate, F.; Naoi, K. Electrolyte systems for high withstand voltage and durability I. Linear sulfones for electric double-layer capacitors. *J. Electrochem. Soc.* **2011**, *158* (8), A872.

(39) Freitag, M.; Giordano, F.; Yang, W.; Pazoki, M.; Hao, Y.; Zietz, B.; Grätzel, M.; Hagfeldt, A.; Boschloo, G. Copper phenanthroline as a fast and high-performance redox mediator for dye-sensitized solar cells. *J. Phys. Chem. C* **2016**, *120* (18), 9595–9603.

(40) Hara, K.; Horiguchi, T.; Kinoshita, T.; Sayama, K.; Arakawa, H. Influence of electrolytes on the photovoltaic performance of organic

dye-sensitized nanocrystalline TiO₂ solar cells. *Sol. Energy Mater. Sol. Cells* **2001**, *70* (2), 151–161.

(41) Yu, Q.; Wang, Y.; Yi, Z.; Zu, N.; Zhang, J.; Zhang, M.; Wang, P. High-efficiency dye-sensitized solar cells: the influence of lithium ions on exciton dissociation, charge recombination, and surface states. *ACS Nano* **2010**, *4* (10), 6032–8.

(42) Haque, S. A.; Tachibana, Y.; Willis, R. L.; Moser, J. E.; Grätzel, M.; Klug, D. R.; Durrant, J. R. Parameters Influencing Charge Recombination Kinetics in Dye-Sensitized Nanocrystalline Titanium Dioxide Films. *J. Phys. Chem. B* **2000**, *104* (3), 538–547.

(43) González-Pedro, V.; Xu, X.; Mora-Sero, I.; Bisquert, J. Modeling high-efficiency quantum dot sensitized solar cells. *ACS Nano* **2010**, *4* (10), 5783–5790.

(44) Guillén, E.; Peter, L. M.; Anta, J. A. Electron Transport and Recombination in ZnO-Based Dye-Sensitized Solar Cells. *J. Phys. Chem. C* **2011**, *115* (45), 22622–22632.

(45) Fürer, S. O.; Milhuisen, R. A.; Kashif, M. K.; Raga, S. R.; Acharya, S. S.; Forsyth, C.; Liu, M.; Frazer, L.; Duffy, N. W.; Ohlin, C. A.; Funston, A. M.; Tachibana, Y.; Bach, U. The Performance-Determining Role of Lewis Bases in Dye-Sensitized Solar Cells Employing Copper-Bisphenanthroline Redox Mediators. *Adv. Energy Mater.* **2020**, *10* (37), 2002067.

(46) Boschloo, G.; Hagfeldt, A. Photoinduced absorption spectroscopy as a tool in the study of dye-sensitized solar cells. *Inorg. Chim. Acta* **2008**, *361* (3), 729–734.

(47) Ardo, S.; Sun, Y.; Staniszewski, A.; Castellano, F. N.; Meyer, G. J. Stark Effects after Excited-State Interfacial Electron Transfer at Sensitized TiO₂ Nanocrystallites. *J. Am. Chem. Soc.* **2010**, *132* (19), 6696–6709.

(48) Cappel, U. B.; Feldt, S. M.; Schöneboom, J.; Hagfeldt, A.; Boschloo, G. The Influence of Local Electric Fields on Photoinduced Absorption in Dye-Sensitized Solar Cells. *J. Am. Chem. Soc.* **2010**, *132* (26), 9096–9101.

(49) Chen, L. X.; Shaw, G. B.; Novozhilova, I.; Liu, T.; Jennings, G.; Attenkofer, K.; Meyer, G. J.; Coppens, P. MLCT State Structure and Dynamics of a Copper(I) Diimine Complex Characterized by Pump-Probe X-ray and Laser Spectroscopies and DFT Calculations. *J. Am. Chem. Soc.* **2003**, *125* (23), 7022–7034.